Soft Matter

In situ transmission electron microscopy observation of the deformation and fracture processes of an epoxy/silica nanocomposite

Journal:	*Soft Matter*
Manuscript ID	SM-COM-10-2021-001452.R1
Article Type:	Communication
Date Submitted by the Author:	09-Dec-2021
Complete List of Authors:	Wang, Pangpang; Institute of Systems Information Technologies and Nanotechnologies, Materials Open Lab. Maeda, Ryusei; Mechanical Design & Analysis Co. Aoki, Mika; Kyushu University, Center for Polymer Interface and Molecular Adhesion Science Kubozono, Tatsuya; Institute of Systems Information Technologies and Nanotechnologies, Materials Open Lab. Yoshihara, Daisuke; Institute of Systems Information Technologies and Nanotechnologies, Materials Open Lab. Shundo, Atsuomi; Kyushu University, Applied Chemistry Kobayashi, Takaya; Mechanical Design & Analysis Co. Yamamoto, Satoru; Kyushu University, Center for Polymer Interface and Molecular Adhesion Science Tanaka, Keiji; Kyushu University, Applied Chemistry Yamada, Sunao ; Institute of Systems Information Technologies and Nanotechnologies

COMMUNICATION

In situ transmission electron microscopy observation of the deformation and fracture processes of an epoxy/silica nanocomposite

Received 00th January 20xx,
Accepted 00th January 20xx

DOI: 10.1039/x0xx00000x

Pangpang Wang, *[a] Ryusei Maeda, [b, ‡] Mika Aoki, [c, ‡] Tatsuya Kubozono, [a] Daisuke Yoshihara, [a] Atsuomi Shundo, [d] Takaya Kobayashi, [b] Satoru Yamamoto, [c] Keiji Tanaka [c, d] and Sunao Yamada *[a]

Herein, we report the *in situ* transmission electron microscopy observation of the deformation and fracture processes of an epoxy resin thin film containing silica nanoparticles under tensile strain. Under tensile strain, the dispersed silica nanoparticles in the composite arrest the progress of the crack tip and prevent crack propagation. Concomitantly, the generation and growth of nanovoids at the epoxy matrix/nanoparticle interfaces were clearly observed, particularly in region near the crack tip. These nanovoids contribute to the dissipation of fracture energy, thereby enhancing the fracture toughness. We also analyzed the local distributions of the true strain and strain rate in the nanocomposite film during tensile testing using the digital image correlation method. In the region around the crack tip, the strain rate increased by 3 to 10 times compared to the average of the entire test specimen. However, the presence of large filler particles in the growing crack suppressed the generation of strain, potentially contributing to hindering crack growth.

Epoxy resins, which are based on formation of networks between epoxy and amine compounds *via* curing reactions, are an important class of thermoset resins. Since epoxy resins are generally in a glassy state under ambient conditions,[1, 2] epoxy resins are usually brittle, which is a critical drawback in resins used as structural materials.[3, 4] One common approach to overcoming this issue is to disperse soft particles into the epoxy matrix as a filler.[5–8] For example, incorporating rubbery polymer particles can remarkably improve the toughness of the epoxy resin because of the energy dissipation induced by the viscoelastic feature of the particles.[6, 7] A similar improvement in toughness has also been reported for epoxy composites containing hard particles such as silica particles.[9–15] However, the toughening mechanism, which should differ from that for soft particles, is not yet clear.

Recently, it has been reported that the physical properties of epoxy resins are much different at the solid, or hard, interface than in the internal bulk region.[16] This may be because the chemical composition of the epoxy resin is heterogeneous along the direction normal to the interface.[17, 18] In addition, the initial reactions of the epoxy and amine components occur more slowly near the substrate than in the bulk region.[19] This leads to a different epoxy network structure and, in turn, different mechanical properties in close proximity to the interface. Thus, to obtain a better understanding of the toughening mechanism in epoxy composites, the deformation process of the resin near filler particles should be examined as a first step.

Herein, we used *in situ* transmission electron microscopy (TEM) to study the deformation and fracture processes of a glassy epoxy film containing independently dispersed silica nanoparticles during the stretching process.[20–22] We first confirmed the wide area of deformation for the epoxy nanocomposite film in which a crack propagated. This enabled us to evaluate (1) how a silica nanoparticle affected crack propagation and (2) how a nanovoid was formed in close proximity to the epoxy/silica interface. In addition, using digital image correlation (DIC),[23] the true strain distribution and the heterogeneous deformation process of the epoxy film under tensile strain was two-dimensionally mapped. This made it possible to show how a single filler particle retained the strain induced by the crack tip.

Hydrogenated bisphenol A diglycidyl ether (HDGEBA), which was used as an epoxy resin, was supplied by New Japan Chemical Co., Ltd. (Japan). 1,4-Cyclohexanebis(methylamine) (CBMA), which was used as a curing agent, was purchased from Tokyo Chemical Industry Co., Ltd. (Japan). Silica nanoparticles with nominal diameters of 50 nm and surfaces treated with phenyl-type silane were supplied by Admatechs Co., Ltd. (Japan) for use as a filler. Pullulan, which was used as a sacrificial layer between the solid substrate and the epoxy layer, was purchased from Tokyo Chemical Industry Co., Ltd. (Japan). Stabilizer-free tetrahydrofuran (THF) was purchased

[a] *Materials Open Lab., Institute of Systems, Information Technologies and Nanotechnologies, Fukuoka 814-0001, Japan.*
[b] *Mechanical Design & Analysis Co., Tokyo 182-0024, Japan.*
[c] *Centre for Polymer Interface and Molecular Adhesion Science, Kyushu University, Fukuoka 819-0395, Japan.*
[d] *Department of Applied Chemistry, Kyushu University, Fukuoka 819-0395, Japan.*
†Electronic Supplementary Information (ESI) available: [A movie of tensile test]. See DOI: 10.1039/x0xx00000x
‡ These authors contributed equally to this work. They should thus be considered co-first authors.

from Wako Pure Chemical Industries, Co. (Japan) and used as a solvent to prepare the mixed dispersion of epoxy resin and silica nanoparticles. Silicon substrates with dimensions of 10 mm × 10 mm were purchased from SAMCO Co., Ltd. (Japan) and washed with piranha solution (H_2SO_4: H_2O_2 = 7: 3 vol/vol) at 363 K for over 2 h before use.

The preparation process of the nanocomposite thin film is shown in Figure S1 (see Supporting Information). First, a 40-nm-thick pullulan film was prepared from a 2.5 wt% aqueous solution on a silicon substrate *via* spin-coating at a speed of 3,000 rpm for 60 s. The film was then dried in a vacuum desiccator for over 12 h before use. Meanwhile, HDGEBA and CBMA (2: 1 mol/mol) were mixed and pre-cured at 373 K for 9 min to obtain a transparent mixture in which the reaction ratio of HDGEBA to CBMA was approximately 65%.[24] Next, a suspension of the silica nanoparticles (1 wt%) in THF was added into the epoxy mixture, and the weight ratio of epoxy resin to silica nanoparticles was tuned to 95: 5. This ratio was sufficient to obtain a nanoparticle dispersion with a low degree of aggregate formation, as verified by TEM observation (*vide infra*). The mixture of epoxy resin and silica nanoparticles was then spin-coated on the top of the pullulan layer at a speed of 3,000 rpm for 60 s. The sample was further heated at 373 K for 24 h under vacuum to reach a fully cured state. The thickness and microstructure of the nanocomposite thin film were confirmed by cross-sectional scanning electron microscopy (SEM; Helios NanoLab 600i, Thermo Fisher Scientific, US).

The nanocomposite thin film prepared on the silicon substrate was cut into pieces with dimensions of 10 mm × 0.5 mm using a razor blade. The sacrificial pullulan layer was dissolved by immersing the silicon/pullulan/nanocomposite sample in water; the free-standing nanocomposite thin film then floated up to water surface. Finally, the floating film was scooped up onto the 20-μm-wide slit of a tensile cartridge (*vide infra*) and stored in a vacuum desiccator.

The cartridge with the sample film was mounted on a TEM holder for tensile testing (Mel-Build Co., Japan). The tensile direction was perpendicular to the slit of the cartridge. The tensile speed of the cartridge was set at 20 nm·s^{-1}. TEM observation was conducted at an accelerating voltage of 80 kV (JEM1400plus, JEOL Ltd., Japan). The exposure time of the charge-coupled device camera mounted in the transmission electron microscope was set to 200 ms to obtain TEM images continuously during stretching. We used a smartphone camera (iPhone 8plus, Apple Inc., US) to capture the monitor display and make a movie at 30 frames per second.

The strain distribution within a region of interest (957 × 696 pixels, approximately 4.9 nm·pixel^{-1}) in the successive TEM images was analyzed by DIC (VIC-2D-v6, Correlated Solutions, US). The measurement conditions of the TEM images were carefully tuned to allow DIC analysis while maintaining the precision of the strain distribution. The important considerations were obtaining a satisfactorily high contrast between the epoxy matrix and the silica nanoparticles and reducing unwanted flickering in the epoxy matrix. The luminance values of the region of interest in a TEM image were converted to discrete values to construct random luminance patterns. A two-dimensional displacement map was obtained by calculating the geometric correlation of the random luminance patterns. The strain (so-called true strain) values were then calculated from the derivation of the displacement.

In general, DIC analysis calculates the displacement field based on the unloaded condition. However, DIC observation in a TEM environment has the following restrictions: (1) it takes a considerable amount of time, both optically and mechanically, from the zero-load state to the steady tensile state; (2) it is necessary to search the target region on the nanometer scale during TEM observation (for example, to find the region near the crack tip); and (3) because of the high magnification of TEM observation, there may be drifts in the TEM images due to changes in the gripping state of the specimen, unavoidable progression of the curing reaction, and so on. Therefore, we extracted a specific period of time (a movie with a length of 2 min, 7 s, Movie S1, see Supporting Information) from the entire TEM image movie of the tensile test and used it for DIC analysis.

Figure S2(a) shows a cross-sectional SEM image of the nanocomposite film spin-coated on a silicon/pullulan substrate (see Figure S1). The upper nanocomposite layer and the lower pullulan layer could be clearly distinguished from each other, and the thickness of the nanocomposite film and pullulan layer were approximately 110 and 40 nm, respectively. In addition, two silica nanoparticles that existed separately in the epoxy resin were observed, implying that the silica nanoparticles were well dispersed in the resin. Figure S2(b) shows a top-view SEM image of the nanocomposite film that had been transferred onto the slit of a tensile cartridge. The film on the 20-μm-wide slit was elongated along the direction perpendicular to the slit. A crack at the left edge of the film advanced toward the right side of the film as tensile strain was applied. Figure S2(c) shows a TEM image of the free-standing nanocomposite thin film transferred onto the tensile cartridge. The silica nanoparticles were well dispersed with a tiny amount of aggregation. Although the size distribution of the silica nanoparticles was somewhat broad, the nominal diameter was approximately 50 nm.

In situ TEM observation of the nanocomposite film during the tensile test was carried out to approximately 2 min (Movie S1, see Supporting Information). A pre-existing crack tip advanced from the left side of the film to the right side. Figures 1(a)–(h) show TEM images acquired at different times from zero [00:00, (a)] to 2 min, 5 s [02:05, (h)]. The number on each picture indicates the elapsed time in minutes and seconds from the start of imaging. In Figure 1(a), the crack tip is not seen in the observation region. In Figure 1(b), the crack tip appears at the left edge of the observation region (blue arrow). As shown in Figures 1(c) and (d), the propagation of the crack was apparently suppressed, and the crack tip expanded along the tensile direction. At the same time, a couple of nanovoids appeared in close proximity to the top and bottom interfacial regions around the silica nanoparticles, as described later. Subsequently, a new crack [indicated by a

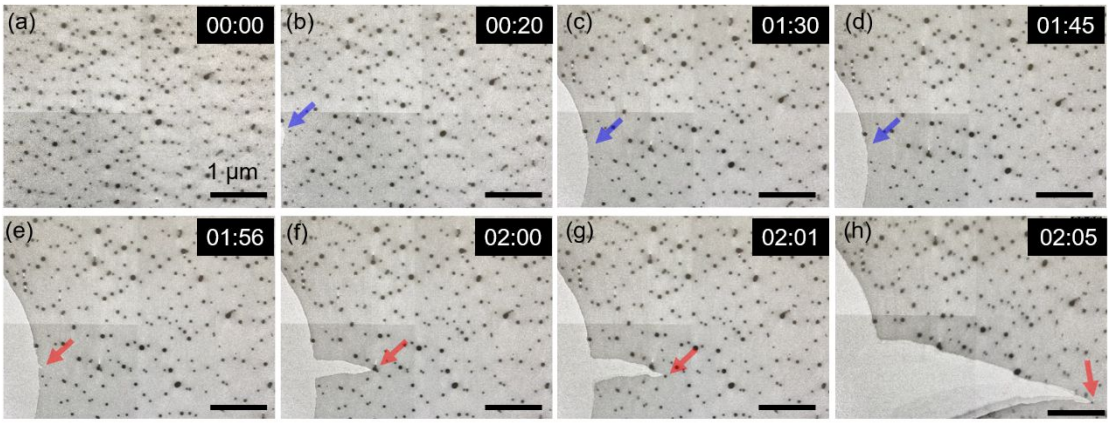

Figure 1. TEM images extracted from the movie of the tensile test. (a) The crack tip is not seen in the observation region. (b) A crack tip appears at the left edge of the observation region (blue arrow). (c), (d) The crack tip becomes rounded due to creep. (e) A new crack tip is generated (red arrow). (f)–(h) The new crack tip grows and is repeatedly arrested when it encounters silica nanoparticles. For practical convenience, the time corresponding to (a) is set to zero (minutes: seconds = 00:00). The time of each image is given in the top-right corner of the image. Scale bars: 1 μm.

red arrow in Figure 1(e)] appeared and propagated toward the right side of the film. The new crack tip encountered a silica nanoparticle ahead of it [Figure 1(f)]. It was difficult at this stage to forecast the appearance point of a new crack. In this case, the crack did not expand; rather, it passed through the bottom side of the particle. Subsequently, the crack tip encountered another silica nanoparticle [Figure 1(g)]. Unlike in the previous case, the crack tip passed through the top side of the particle and again encountered another nanoparticle [Figure 1(h)].

Figure 2 shows two magnified TEM images showing the crack expansion at (a) 0 min, 20 s (00:20) and (b) 1 min, 30 s (01:30) before the formation of a new crack. Nanovoids (marked by arrows in the images) around the silica nanoparticles were much more numerous at 1 min, 30 s (01:30) than at 0 min, 20 s (00:20), indicating that the nanovoid formation probability increased as the tensile test proceeded. In addition, the nanovoids that appeared in the vicinity of the crack tip grew quickly as the tensile test proceeded. The formation and growth of nanovoids retarded the formation of new cracks and increased the fracture toughness of the resin, even in close proximity to the crack tip. The nanovoids formed easily at the two poles of the silica nanoparticles and between two adjacent nanoparticles, where stress was concentrated.

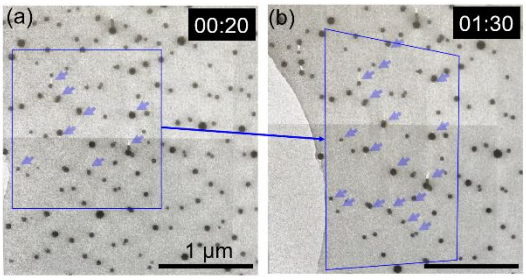

Figure 2. Nanovoids formed at the interfaces between silica nanoparticles and the epoxy matrix under different strain states. The region indicated by the blue rectangle in (a) (time = 00:20) changed into that in (b) (time = 01:30) as the tensile test proceeded. The formed nanovoids are indicated by light-blue arrows. Scale bars: 1 μm.

Another possible reason for nanovoid formation may be the different chemical composition (or cure state) in the epoxy resin compared to at the epoxy/silica interface [16–18], causing the nanocomposite to be easily fractured at the interfaces.

As described above, the propagation of the crack was suppressed in the region shown in Figures 1(a)–(d). Thus, we carried out DIC analysis in this region. Figure 3 shows the contour plots of the true strain along the y-axis. These contour plots were generated every 12 s. The deformation of the nanocomposite film was clearly non-uniform, and the strain constraint was remarkable, particularly in the region where the filler was dense or the particle size was large.

Figure 4(a) shows the true strain curves along the white dashed line in each contour plot shown in Figure 3. The left end of the path is positioned close to the crack tip, where the maximum strain reached 0.6. The overall strain level increased over time because the tensile load was continuously applied, and the strain decreased as the distance from the crack tip increased. The imaging region was carefully selected to observe the effect of strain constraint by the filler. In Figure 4(a), a filler particle with a diameter of approximately 100 nm is located approximately 2,500 nm from the crack tip. The strain in the vicinity of this filler particle is 0.1 or less, and a region with small strain is observed in the area within approximately 100 nm from the filler particle's surface. The presence of a filler with such an effect on crack propagation may contribute to hindering crack growth. Figure 4(b) shows the curves of strain rate. The strain rate was simply obtained by dividing the true strain at each time by the elapsed time from time zero. As mentioned above, the strain values shown in Figure 3 and Figure 4(a) do not include the strain that occurred before the first image was taken, but the strain rate calculated from the increment of true strain is quantitative.

In this study, a tensile rate of 20 nm·s^{-1} was applied to a test specimen with a length of 20 μm, so the average strain rate was expected to be approximately 1.0 × 10^{-3} s^{-1}. On the other

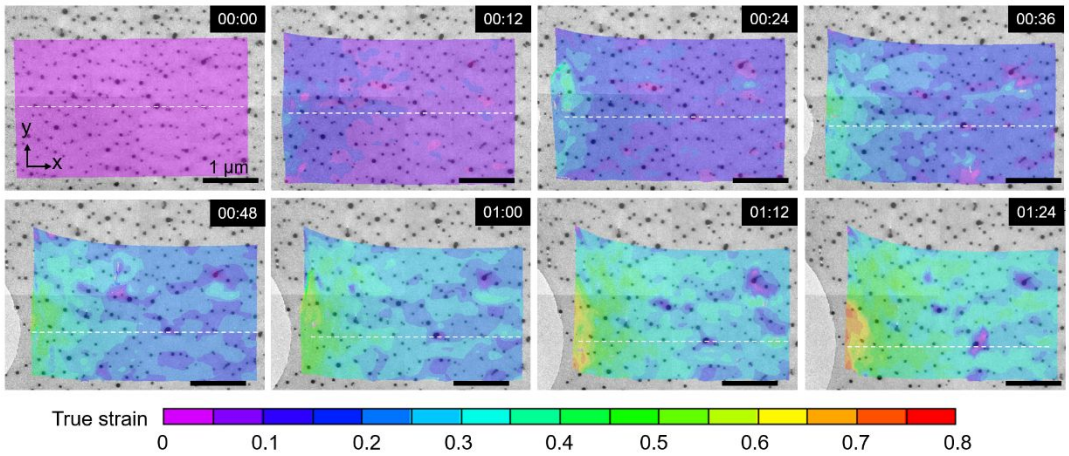

Figure 3. True strain distributions in the vicinity of the crack tip. The true strain in the upper-left figure is assumed to be zero. Tensile displacement was applied continuously at a rate of 20 nm·s^{-1} in the y direction. The crack was expected to grow in the x direction. The true strain and strain rate along the white dashed line shown in each image are shown in Figure 4.

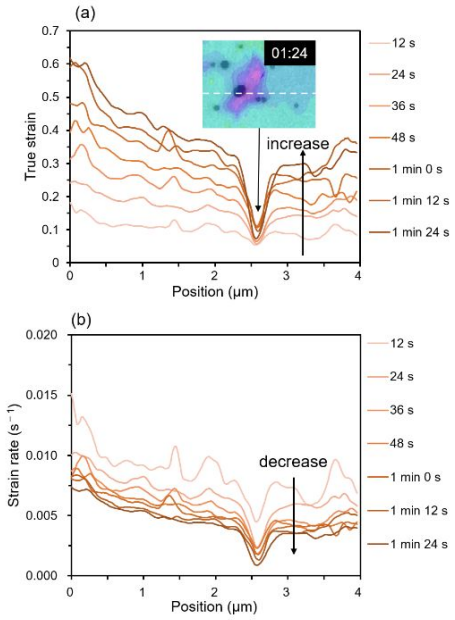

Figure 4. (a) True strain distributions along the y-axis under different tensile states (from 0 min, 12 s to 1 min, 24 s). Due to the presence of a large filler particle located approximately 2,500 nm from the crack tip, the generation of strain was constrained. (b) Calculated strain rates along the y-axis.

hand, in Figure 4(b), strain rates ranging from 3.0 × 10^{-3} to 1.0 × 10^{-2} s^{-1} are observed. Thus, the strain rate in the region around the crack tip was 3 to 10 times higher than the average strain rate of the entire test specimen. Due to the presence of the large particles mentioned above, the strain rate in the vicinity of the particles was limited to a value below the average strain rate. Additional microscopic evaluations are planned for the future.

On the other hand, as shown in Figures 5(a)–(d), which respectively show the same regions as Figures 1(e)–(h), a new crack appeared, and the crack tip propagated toward the right, where it encountered silica nanoparticles. We analyzed the velocity of crack propagation as a function of the distance between the crack tip and the left edge of the film before crack formation along the direction of crack propagation. The velocity curve is shown in Figure 5(e). The new crack propagated in the epoxy matrix with a velocity of approximately 0.5–7.6 μm·s^{-1}. However, the velocity decreased to less than 0.1 μm·s^{-1} when the crack tip encountered a silica nanoparticle. The inset of Figure 5(e) presents magnified TEM images showing the suppression of crack-tip propagation in the vicinity of a silica nanoparticle (the same large nanoparticle depicted in Figure 4). Slow crack propagation was also observed on the nanometer scale. These results indicate that the silica nanoparticles effectively suppressed the propagation of the crack tip.

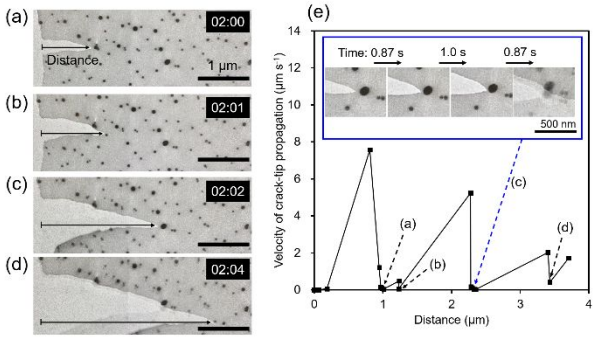

Figure 5. (a)–(d) TEM images of cracks propagating toward the right. The crack tips are arrested when they encounter silica nanoparticles. (e) The velocity of crack propagation as a function of the distance between the crack tip and the left edge of the film before crack formation. The insets in (e) show magnified TEM images of a crack suppressed by a silica nanoparticle. The time intervals between two sequential TEM images are also shown.

Conclusions

We conducted tensile tests of epoxy/silica nanocomposite thin films in a transmission electron microscope and achieved the

in situ observation of the deformation and fracture processes of the films on the nanoscale. We clearly observed the arrest of the crack tip by dispersed silica nanoparticles, which decreased the velocity of crack propagation. In addition, the generation of nanovoids around the silica nanoparticles assisted in distributing the tensile energy in the epoxy matrix, which contributed to enhancing the fracture toughness. The true strain and strain rate distribution analyzed by DIC provided a much clearer image of the deformation of the composite film. This visualization of the deformation and fracture processes of the nanocomposite film on the nanoscale is helpful to unravel the mechanism of enhanced polymer fracture toughness upon the incorporation of nano-fillers, especially the fillers' shapes and concentrations. Ongoing work is focused on comparing the fracture toughness of the nanocomposite thin film with that of its bulk counterpart, which is also important.

Author Contributions

Pangpang Wang conducted the tensile test of the nanocomposite film and wrote the manuscript. Mika Aoki prepared the epoxy/silica nanocomposite thin film. Ryusei Maeda analyzed the strain distribution in the film by DIC. Tatsuya Kubozono and Daisuke Yoshihara helped prepare the sample for the tensile test. Atsuomi Shundo investigated the curing condition of the epoxy resin. Satoru Yamamoto discussed the deformation mechanism of the epoxy resin at the molecular level. Takaya Kobayashi analyzed the DIC results. Keiji Tanaka and Sunao Yamada supervised the entire study.

Conflicts of interest

There are no conflicts to declare.

Acknowledgements

This work was supported by the JST-Mirai Program (Grant Number JPMJMI18A2). The authors thank New Japan Chemical Co., Ltd. for supplying the epoxy resin, Admatechs Co., Ltd. for supplying the silica nanoparticles, and the Analysis Centre of Fukuoka Industry-Academia Symphonicity for facility support.

References

1 J. K. Lee and J. Y. Hwang. *Polym. J.*, 2003, **35**, 191.
2 A. Shundo, M. Aoki, S. Yamamoto and K. Tanaka, *Macromolecules*, 2021, **54**, 5950.
3 G. Levita, S. De Petris, A. Marchetti and A. Lazzeri, *J. Mater. Sci.*, 1991, **26**, 2348.
4 M. Aoki, A. Shundo, S. Yamamoto and K. Tanaka, *Soft Matter*, 2020, **16**, 7470.
5 A. F. Yee and R. A. Pearson, *J. Mater. Sci.*, 1986, **21**, 2462.
6 Y. Huang and A. J. Kinloch, *J. Mater. Sci. Lett.*, 1992, **11**, 484.
7 H. R. Azimi, R. A. Pearson and R. W. Hertzberg, *J. Mater. Sci.*, 1996, **31**, 3777.
8 J. H. Hodgkin, G. P. Simon and R. J. Varley, *J. Polym. Adv. Technol.*, 1998, **9**, 3.
9 Y. Nakamura and M. Yamaguchi, *Polymer*, 1992, **33**, 3415.
10 B. B. Johnsen, A. J. Kinloch AJ, R. D. Mohammed, A. C. Taylor and S. Sprenger, *Polymer*, 2007, **48**, 530.
11 H. Liu, G. Wang, Y. Mai and Y. Zeng, *Composites Part B*, 2011, **42**, 2170.
12 P. Dittanet and R. A. Pearson, *Polymer*, 2012, **53**, 1890.
13 Q. Meng, C. Wang, N. Saber, H. Kuan, J. Dai, K. Friedrich and J. Ma, *Mater. Des.*, 2014, **61**, 75.
14 C. R. Picu, K. K. Krawczyk, Z. Wang, H. Pishvazadeh-Moghaddam, M. Sieberer, A. Lassnig, W. Kern, A. Hadar and D. M. Constantinescu, *Composites Sci. & Technol.*, 2019, **183**, 107799.
15 A. Dadrasi, G. A. Farzi, M. Shariati, S. Fooladpanjeh and V. Parvaneh, *Eng. Fract. Mech.*, 2020, **232**, 107047.
16 J. Chung, M. Munz and H. Sturm, *Surf. Interface Anal.*, 2007, **39**, 624.
17 M. Aoki, A. Shundo, K. Okamoto, T. Ganbe and K. Tanaka, *Polym. J.*, 2019, *51*, 359.
18 S. Yamamoto, R. Kuwahara, M. Aoki, A. Shundo and K. Tanaka, *ACS Appl. Polym. Mater.*, 2020, **2**, 1474.
19 T. Hirai, K. Kawasaki and K. Tanaka, *Phys. Chem. Chem. Phys.*, 2012, **14**, 13532.
20 G. H. Michler and H. K. von Schmeling, *Polymer*, 2013, **54**, 3131.
21 T. Higuchi, T. Gondo, H. Miyazaki, A. Kumagai, K. Akutagawa and H. Jinnai, *Microscopy*, 2018, **67**, 296.
22 T. Miyata, T. Nagao, D. Watanabe, A. Kumagai, K. Akutagawa, H. Morita and H. Jinnai, *ACS Appl. Nano Mater.*, 2021, **12**, 4452.
23 K. E. Yazzie, J. J. Williams, D. Kingsbury, P. Peralta, H. Jiang and N. Chawla, *JOM*, 2010, **62**, 16.
24 M. Aoki, A. Shundo, R. Kuwahara, S. Yamamoto and K. Tanaka, *Macromolecules*, 2019, **52**, 2075.